Multipolar SPM machines for direct drive application: a general design approach

Multipolar SPM machines for direct drive application: a general design approach

B. Boazzo, G. Pellegrino, A. Vagati
Politecnico di Torino
Corso Duca degli Abruzzi 24, Torino, 10129 Italy

***Abstract* - A closed-form, per-unit formulation for the design of surface mounted permanent magnet motors having high numbers of poles is hereby proposed. The analytical expression of machine inductances is presented, covering distributed and concentrated windings configurations. The paper addresses how the slot/pole combination, the geometric variables and the number of poles are related to average torque, the Joule loss and the power factor. The performance of distributed and concentrated windings machines is compared analytically, in normalized quantities. Last, the design approach is tested on four design examples, including all winding types and validated by finite element analysis.**

Index Terms – PM motor drives, PM machines, Motor Design, Surface Mounted PM machines, Wind turbines.

I. INTRODUCTION

Permanent magnet (PM) synchronous machines are recognized for their performance in terms of torque density and efficiency. In particular, direct-drive machines of the surface mounted PM type (SPM) have been increasingly adopted as motor and/or generators in many up to date applications such as traction and propulsion, aerospace and energy production from renewable resources [1]. Recently, the price of rare earth PMs have suffered from a significant volatility, yet the interest for PM based electrical machines is high, as recent works demonstrate [1-2].

Over the last decade, a lot of effort has been devoted to the investigation of fractional slots per pole per phase combinations and concentrated windings, for their better fault tolerance, ease of manufacturing, short end connections and high copper filling factor [2-10]. However, distributed winding machines are still adopted in many direct drive applications.

The paper proposes a general, per-unit design approach for three-phase SPM machines for direct-drive applications. The investigation covers distributed and concentrated winding types; it is based on simple analytical formulas, valid for all integer and fractional slot numbers. The elementary block reported in Fig. 1 represents one pole of a SPM machine, e.g. with distributed windings. A rotating, direct-drive SPM machine with a high number of poles is the assembly of a proper number of such poles, with very good accuracy.

The key-geometric parameters, defined in Fig. 1, are the pole pitch a, the tooth length l_t and the PM length l_m. In all formulas, they will be normalized by the airgap length g. Another very important parameter is the number of slots per pole per phase q, that is an integer for distributed windings and a fraction for concentrated windings. For fractional slot windings a is the rotor pole pitch. Other variables (k_m, B_{fe}, k_t) are defined in Fig. 1, as a reference for the symbols adopted throughout the paper.

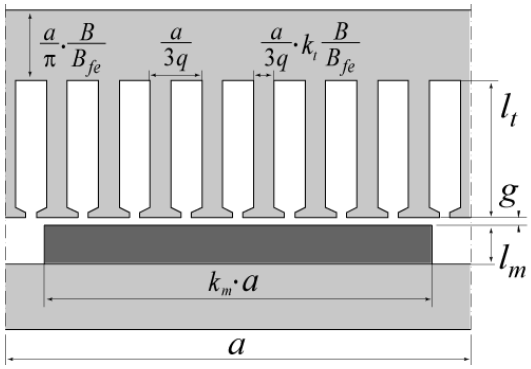

Figure 1. Elementary block of linear-like SPM synchronous machine, corresponding to one PM pole pitch. The example has q = 3 slots per pole per phase.

Key figures of merit such as the shear stress (related to torque density), the power factor (PF) and the Joule loss per outer surface unit will be expressed as a function of q and the geometric quantities of Fig. 1. Optimal combinations of the design variables are addressed, given the type of windings (concentrated, distributed) and the cooling setup (Joule loss per square meter). Particular emphasis is put on how the PF can be maximized by design, given the shear stress, or vice versa. Such emphasis has the following motivations, that have relevance in particular for fractional slot machines:

- A low power factor negatively affects the size of the power converter.
- A low power factor indicates that the machine can be prone to load-dependent core saturation, leading to a torque reduction.
- The machine inductance is the key design parameter of fractional-slot SPM machines. The paper shows that PF maximization is a powerful criterion for orientating the choice of all other design variables.

After the model is introduced and commented, a design flowchart is proposed and applied to three design examples, one per type of windings. The design examples are validated by Finite Element Analysis (FEA) and the comparison between FEA and the analytical model is commented. General considerations about where and how to use factional slot configurations are given in the final

discussion. This work is the prosecution and development of [11], where the modelling approach was first applied to single layer factional windings only.

II. PER UNIT MACHINE MODEL

A. Magnetic loading

The magnetic loading B is defined as the peak of the fundamental component (wavelength = $2a$), at no load (1).

$$B = \hat{B}_{gap,fund} = k_b \cdot \frac{B_r}{1 + k_c \cdot \frac{g}{l_m}} \qquad (1)$$

Where B_r is the PM remanence, k_c is the Carter coefficient and k_b is a shape factor that quantifies the fundamental harmonic, given the magnets' pole arc [12].

$$k_b = \frac{4}{\pi} \cdot sin\left(k_m \cdot \frac{\pi}{2}\right) \qquad (2)$$

Apart from the Carter coefficient, and given the airgap length, the no-load magnetic loading (1) depends on rotor parameters only and it is ***independent of the rotor pole pitch a***. The effect of steel saturation at load is discussed at subsection VII.B.

Ultimately, the normalized PM thickness l_m/g determines the magnetic loading (1) and also the resistance to de-magnetization of the machine. Over certain values, like l_m/g = 6, it is not convenient to further increase l_m/g to improve B, unless it is required by special overload needs and related demagnetization issues. The formulas relating l_m/g and the de-magnetization limit are not reported because they are out of the scope of this paper. The example value l_m/g = 6 will be used in the following and final designs must be eventually verified against de-magnetization through analysis and FEA.

B. Electric loading and shear stress

The electric loading is defined in (3):

$$A = \frac{3}{2} \cdot \frac{N}{a} \cdot k_w \cdot I_q \qquad (3)$$

Where k_w in (3) is the winding factor, N is the number of conductors in series per pole per phase. I_q is the phase current amplitude. It is implicitly intended that the current vector is aligned with the quadrature axis, that is the maximum force (torque) per Ampere situation. The average shear stress is:

$$\sigma = BA \qquad (4)$$

The shear stress is measured in N/m^2 and it is the time-averaged tangential force acting on the elementary block of Fig. 1, divided by the airgap surface. In case of a cylindrical machine, the shear-stress is proportional to its torque per rotor volume density.

Once the PM grade, shape and thickness are set, the magnetic loading (1) is determined. Then the shear stress will depend on the electric loading (3) only. Its upper limits are either related to Joule loss (i.e. thermal limit or efficiency target) or to the aforementioned de-magnetization.

C. Specific Joule loss

The Joule loss factor k_j (5), expressed in W/m^2, is obtained by dividing the copper loss of the elementary block of Fig.1 per its outer surface, and it is representative of the heat dissipation capability of the machine:

$$k_j = \frac{2\rho_{Cu} k_{end}}{k_{Cu}(1 - k_t \cdot B/B_{fe})} \cdot \left(\frac{A}{k_w}\right)^2 \cdot \frac{1}{l_t} \qquad (5)$$

ρ_{Cu} is the electric resistivity of copper, k_{Cu} is the slot filling factor (net copper over slot cross section), k_{end} is the length of the conductors, including end connections, divided by their active length. B_{fe} is the peak flux density in the stator back iron, that is inversely proportional to the cross section of the stator yoke as defined in Fig. 1. k_t is the tooth scaling factor, also defined in Fig. 1, and it is proportional to the tooth width. As for (1), also the Joule loss factor (5) is independent of the pole pitch, and it is also independent of the airgap lenght. ***In substance, k_j depends on the tooth length***, and the tooth length is not normalized in this case. The value of k_j at continuous conditions basically determines the length of the teeth, that has a direct impact on the mass of the active parts, as will be shown in the next sections.

D. Power factor

The vector diagram referring to one machine pole is reported in Fig. 2. The current vector is in time quadrature with the PM flux linkage ($\lambda_{m,pole}$) and the stator resistance voltage drop is neglected. The PF angle φ can be expressed in normalized quantities as follows:

$$tan\varphi \cong \frac{4\mu_0}{3\pi} \cdot L_{pole,pu} \cdot \frac{A}{B} \qquad (6)$$

Where the subscript "*pu*" stands for per-unit and base for inductance normalization is:

$$L_{base} = \frac{\mu_0 \cdot l}{2} \cdot \left(\frac{2}{\pi} \cdot k_w \cdot N\right)^2 \qquad (7)$$

being l the stack length. According to (6), the power factor is determined by the per-unit inductance $L_{pole,pu}$ only, once the shear stress and its components B and A are given.

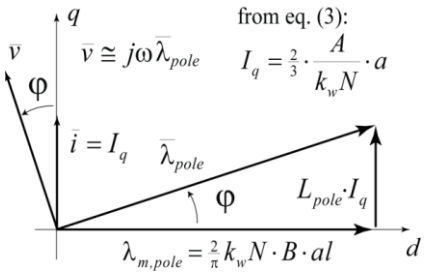

Figure 2. Definition of the power factor angle φ (6).

Provided that rare earth magnets are used, the factor B

has very little variations when changing from one machine to another, and then ***the per unit inductance directly relates the power factor to the shear stress (torque density).*** This is of little importance with distributed windings, but it can become critical for fractional slot machines, in particular the single layer ones, where wrong design choices can lead to impractical values of the power factor. In the following the minimization of the pole per-unit inductance is addressed, along with the criteria for a best compromise between shear stress and power factor.

III. ANALYSIS OF THE PER-UNIT INDUCTANCE

The inductance of the elementary block of Fig. 1 is the sum of the *slot leakage* and the *air gap* inductances:

$$L_{pole,pu} = L_{g,pu} + L_{slot,pu} \qquad (8)$$

In normalized quantities, the two components of (8) depend on the geometric variables defined in Fig. 1, with expressions that are different for distributed (integer q) and concentrated (fractional q) windings.

A. Distributed winding machines

The magnetization inductance is given by (9):

$$L_{g,pu} = \frac{\pi^2}{6 \cdot k_w^2} \cdot \left(\frac{1}{k_c + \frac{l_m}{g}} \right) \cdot \frac{a}{g} \qquad (9)$$

The slot inductance expression is (10):

$$L_{slot,pu} = \frac{\pi^2}{2k_w^2} \cdot \frac{\frac{l_t}{g}}{\left(1 - \frac{B}{B_{fe}} k_t\right)} \cdot \left(\frac{a}{g}\right)^{-1} \qquad (10)$$

Expressions (9) and (10) are reported for q = 1 only for simplicity and because most of machines with many poles have q = 1, as also the design example at Section VI. The equations could be complicated to include q > 1 and short-pitching. The results for q = 2, full pitch, are reported in the graphs of Figs. 4-7 for the sake of comparison with q = 1, showing little difference at the purposes of this analysis.

From (9) it turns out that L_g is proportional to the ratio a/g. Conversely, if the tooth length to airgap rate l_t/g is fixed, then L_{slot} is inversely proportional to a/g, as put in evidence in (10)[1].

The dashed curves in Fig. 2 show that the per-unit inductance, sum of (9) and (10), has a minimum for a precise a/g value. It can be demonstrated that the minimum inductance condition is when $L_g = L_{slot}$. Posing $L_g = L_{slot}$, the pole pitch to air gap ratio that minimizes the inductance is found:

$$\left(\frac{a}{g}\right)_{Lmin} = \sqrt{\frac{3 \cdot \frac{l_t}{g}\left(1 + \frac{l_m}{g}\right)}{1 - \frac{B}{B_{fe}} k_t}} \qquad (11)$$

The minimum inductance, corresponding to (11), is:

$$\left(L_{pole,pu}\right)_{min} = \frac{\pi^2}{\sqrt{3} k_w^2} \sqrt{\frac{\frac{l_t}{g}}{\left(1 + \frac{l_m}{g}\right) \cdot \left(1 - \frac{B}{B_{fe}} k_t\right)}} \qquad (12)$$

The tooth to airgap length ratio l_t/g has effects on (11) and (12), as can be also seen in Fig. 2. The pole pitch (11) depends on l_m/g and l_t/g mostly. Typical values of k_t are 0.8 to 0.9, for distributed windings.

A. Fractional slot machines

The slot inductance expression is (13), where n_l is the number of layers, equal to one for single layer and to two for double layer configurations, respectively. For n_l =1 the expression (13) equals (10).

$$L_{slot,pu} = \frac{\pi^2}{2k_w^2} \cdot \frac{\frac{l_t}{g}}{\left(1 - \frac{B}{B_{fe}} k_t\right)} \cdot \left(1 - \frac{3 \cdot (n_l - 1)}{4 \cdot Q_o}\right) \cdot \left(\frac{a}{g}\right)^{-1} \qquad (13)$$

Q_0 is the number of slots corresponding to half the electrical periodicity of the machine [7], for those q where anti-periodic symmetry conditions apply, or corresponding to the full electrical period, when they do not. In other words, the number Q_0, descending directly from q, represents the minimum number of slots to be simulated when symmetry boundary conditions (anti-periodic or periodic, in case) are adopted. $L_{g,pu}$, either for single or double layer windings is:

$$L_{g,pu} = \frac{1}{n_l} \cdot \frac{\pi^2}{12(q k_w)^2} \cdot \left(\frac{1}{k_c + \frac{l_m}{g}} \right) \cdot \frac{a}{g} \qquad (14)$$

According to the factor $1/n_l$ in (14), ***the air gap inductance of a double layer machine is half the one of the single layer machine having the same geometry***. This conclusion is valid for all values of q. The derivation of (9)-(10) and (13)-(14) is reported in the Appendix.

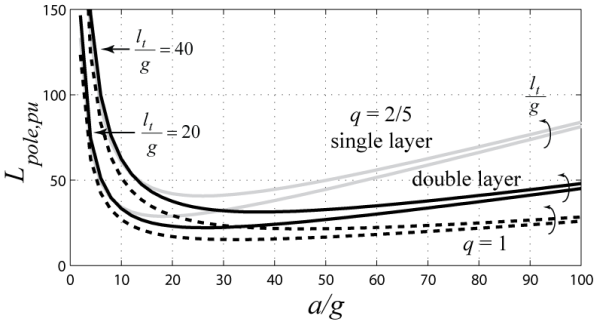

Figure 3. Per-unit inductance versus the pole pitch to airgap ratio. The examples refer to q = 1 and q = 2/5, single and double layer. l_m/g = 6 and l_t/g is a parameter.

In Fig. 3 the per-unit pole inductance is reported as a function of a/g for the example cases q = 1 and q = 2/5, single and double layer. Double layer machines tend to have a lower inductance than single layer ones, as intuitive, and have the minimum inductance condition at larger pole pitch values. The comparison between fractional machines

[1] The airgap can be simplified between l_t/g and $(a/g)^{-1}$ in (10) and (13), meaning the slot inductance is proportional to l_t/a, whatever the airgap. The form of (10) was chosen for having all dimensions normalized by g.

having different q is reported in Fig. 4a, for single layer, and Fig. 4b, for double layer. The two figures also report the curves for integral q, that are all the same, instead, independently from q being one, two or more.

Posing (13) equal to (14), the minimum inductance condition and the minimum inductance value are now:

$$\left(\frac{a}{g}\right)_{Lmin} = q\sqrt{\frac{6n_l\cdot\left(1-\frac{3\cdot(n_l-1)}{4\cdot Q_o}\right)\frac{l_t}{g}\cdot\left(1+\frac{l_m}{g}\right)}{\left(1-\frac{B}{B_{fe}}k_t\right)}} \quad (15)$$

$$\left(L_{pole,pu}\right)_{min} = \frac{1}{q}\cdot\frac{\pi^2}{\sqrt{6}k_w^2}\sqrt{\frac{\frac{l_t}{g}\left(1-\frac{3\cdot(n_l-1)}{4\cdot Q_o}\right)}{n_l\cdot\left(1+\frac{l_m}{g}\right)\cdot\left(1-\frac{B}{B_{fe}}k_t\right)}} \quad (16)$$

The minimum inductance pole pitch (15) is proportional to the fractional q, while it was insensitive to integer q in (11), as also evident from Fig. 4. This accounts for how critical the choice of q can be when designing a fractional slot machine, for keeping the power factor within the limits, as addressed in the following section. Also the minimum inductance value (16) varies a lot from one fractional q to another, that is again verified in Fig. 4.

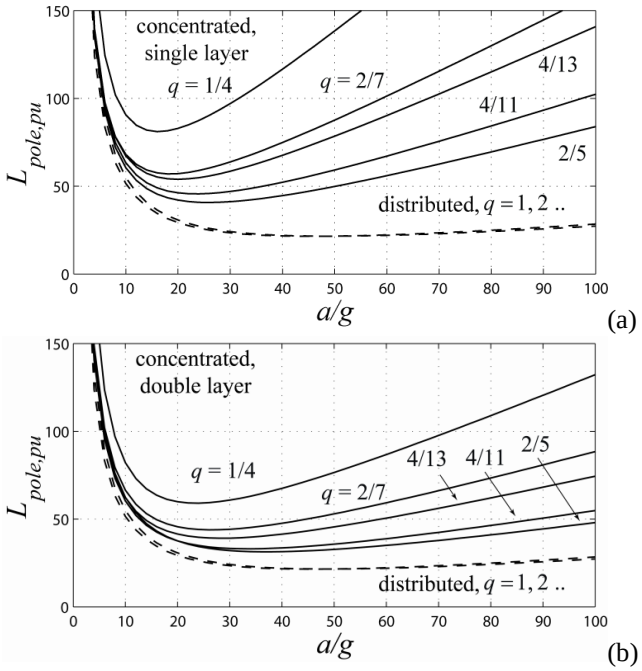

Figure 4. Per-unit inductance for different values of fractional q. a) Single layer machines compared with integral q; b) Double layer machines compared with integral q. All examples have l_m/g = 6 and l_t/g = 40.

IV. MAXIMUM POWER FACTOR MACHINES

Machines having minimized inductance are compared in this section, meaning that their pole pitch satisfies the condition (11), for integral q, and (15) for fractional q, given the tooth length l_t/g. Figure 5 reports the pole pitch as a function of the number of slot per pole per phase. In case of cylindrical machines all having the same rotor diameter, such a/g values are a measure of the number of pole pairs, in inverse proportion. From Fig. 5:

- ***fractional slot machines*** tend to have a smaller $(a/g)_{Lmin}$ and then ***a higher number of poles***, when the minimum inductance criterion is satisfied.
- In such conditions, double layer machines can be close to integral slot ones, for values such as q = 1/2 or 2/5.
- Low q machines and single layer machines are forced to have a high number of poles (low a/g) for keeping the inductance low.

Figure 6 reports the minimum values of the per unit inductance (12) and (16), giving evidence of what anticipated in Figs. 3 and 4:

- integral slot machines are insensitive to q while fractional slot ones are very sensitive to q.
- The minimum inductance is inversely proportional to the fractional q, and becomes very large for little values of q such as 1/8 or 1/10;

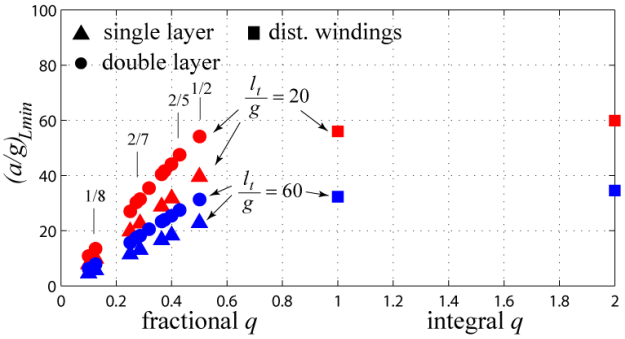

Figure 5. Pole pitch factor that minimizes the machine inductance, as a function of the number of slots per pole per phase. l_t/g is a parameter

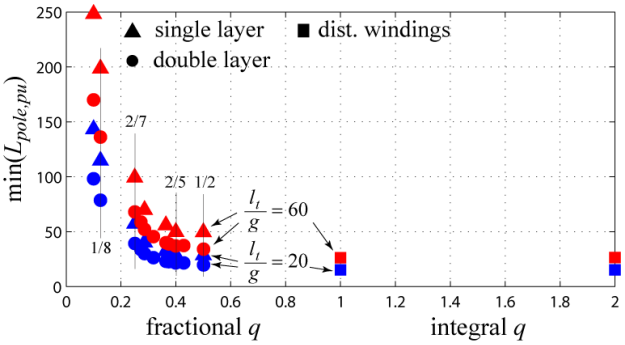

Figure 6. Minimum pole per-unit inductance as a function of the number of slots per pole per phase and the tooth length. l_t/g is a parameter

As said after equation (6), the per-unit inductance determines the power factor given the shear stress. In Fig. 7 machines all having the same shear stress are evaluated, and their maximum PF is reported for all q values, following the pole pitch conditions of Fig. 5 and the minimized inductances of Fig. 6. The shear stress is 62.5 kN/m^2 for all machines, and the corresponding electric loading is 55 kA/m, according to (1) and (4). The power factor is calculated via (6). All the examples of Fig. 7 have the same airgap and rotor parameters (l_m/g = 6, B_r = 1.12 T, k_b = 1.15, that is a typical value).

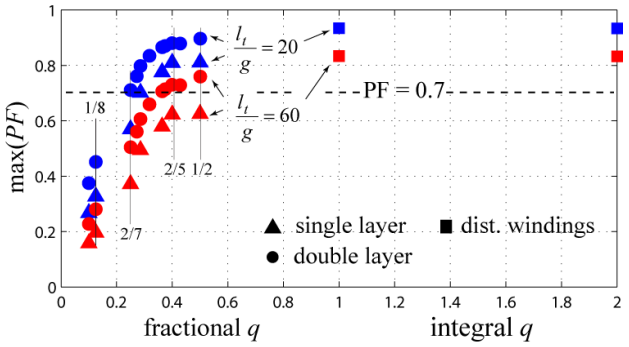

Figure 7. Maximum power factor at given shear stress (σ = 62.5 kN/m^2) as a function of the number of slots per pole per phase and the tooth length. l_t/g is a parameter

The results of Fig. 7 show that:

- With low fractional values of q (e.g. 1/8) there is no way of having an acceptable power factor, even if the pole pitch is chosen for PF maximization.
- Popular slot per pole combinations such as 2/7 are at risk for this reason, with single layer windings.
- Shortening the teeth improves the power factor, but it also directly increases the specific loss (5).
- Therefore, in many cases it is actually impossible to have an acceptable PF with a low fractional q and single layer windings, due to the thermal limit.
- This becomes even more serious when the minimum inductance condition (15) is not respected.
- The PF of integral slot machines is steadily high, and it is then not necessary to optimize the pole pitch, in this case.
- On the contrary, integral slot machines can even have a PF that is too high, and related side effects such as high short circuit currents and PWM current ripple.

V. DESIGN FLOWCHART

This section describes how a rotating machine can be designed via the linear per-unit model developed so far. It is convenient to introduce the relationship between torque and shear stress (17), depending on the rotor radius r and the stack length l, and the expression of the number of poles (18), given the radius and the pole pitch.

$$T = \sigma \cdot 2\pi \cdot \mathrm{r}^2 \cdot \mathrm{l} \qquad (17)$$

$$p = \frac{\pi \cdot \mathrm{r}}{a} \qquad (18)$$

The flowchart is organized as follows: firstly, the elementary block is determined, in terms of size and performance, by applying the per-unit model iteratively according to the design constraints. Then, the rotating machine is obtained as the assembly of a proper number of the just defined blocks. The minimum inductance condition orientates the choice of the pole pitch and then the number of poles (18). When the PF is actually a problem (e.g. single layer machines), then such pole pitch will be the actual design choice, otherwise it is always convenient to reduce the pole pitch for increasing the number of poles and then the mass of the active parts.

It is now assumed that the lower limit to the rated power factor is 0.7, as a reference value, but different choices can be made. Elementary blocks having the PF lower than 0.7 are then rejected and the model is re-evaluated with different inputs.

B. *Preliminary data*

- Airgap length g
- q and type of winding
- PM grade (B_r) and thickness l_m/g
- Steel exploitation B_{fe} (peak)
- Cooling and thermal constraint, represented by the target specific loss k_{j0}
- Target shear stress σ_0, with reference to typical figures of machines having the same type of cooling and the same size.

C. *Design of the elementary block*

1. The magnetic loading B is calculated via (1).
2. The electric loading is calculated from B and the σ_0 target, according to (4).
3. The tooth length is tentatively set according to the loss target k_{j0}, according to (5). The end connection factor is a tentative value in this case, to be recalculated once the active length and the pole pitch are finally done. This can require some iteration.
4. The reference pole pitch $(a/g)_{Lmin}$ is calculated according to the minimum inductance condition, (11) or (15), respectively.
5. The minimized power factor is evaluated and compared to the limit.
   a. ***If the PF is 0.7 or little more, then the block is completely defined***.
   b. If the PF is lower than 0.7, then l_t is reduced and the flowchart is restarted from point 3. One of the two targets σ_0 and k_{j0} must be relaxed, in this case.
   c. If there is a PF margin (PF >> 0.7), then the pole pitch is reduced with respect to $(a/g)_{Lmin}$ for increasing the number of poles, as aforementioned.

The outputs of this stage are:

- the pole pitch a/g and the tooth length l_t/g.
- The shear stress, the power factor, the Joule loss factor.

As said at point 5c, most of the times a PF margin exists and it is not convenient to stay on the minimum inductance pitch. If reducing the pitch still maintains an acceptable PF, it is convenient to do it, because machines with a shorter pitch will have shorter end connections, a lighter back iron and a lower short circuit current. Having a PF margin is very often the case with distributed windings, less often with double layer, fractional q and it is more rare with

single layer windings. In conclusion, ***the $(a/g)_{Lmin}$ sets an upper limit to the pole pitch***: all good machines have a pitch that is equal or lower than that, whilst choosing it larger would only give disadvantages in terms of weight, PF and end connections.

D. Additional input data

The rotating machine is defined according to:

- the target torque T_0 and the rated speed.
- The maximum outer radius (R_0) and stack length (l_0).

E. Design of the rotating machine

Given the shear stress of the elementary block:

1. the product r^2l is evaluated via (17), according to the target torque.
2. From r^2l, the rotor radius and stack length are chosen, within the maximum length limit.
3. The number of pole pairs (18) is calculated and truncated to the closest feasible number. Not all integers are feasible, when dealing with fractional slots.
4. The end connection length is corrected and the specific loss is recalculated according to.
5. Also the machine inductance and the power factor are recalculated, after the pole pair truncation.
6. The stator outer radius is calculated and compared to its limit
   a. ***If the outer radius is ok, then the design is finished.***
   b. If it is too large, the flowchart restarts from point 2 with a reduced r and an increased l, where possible.
   c. If both l and R are over their limits, some constraint must be relaxed.

Once the flowchart is completed, the final design is FEA evaluated.

VI. DESIGN EXAMPLES

The target performance, common to all design examples is the one of a ***direct-drive wind power generator***, rated 3 MW at 16.9 rpm, that means 1695 kNm continuous torque. The target specific loss is k_{j0} = 7500 W/m^2, referring to direct ventilation from the wind and the stator diameter should be lower than or equal to 4 m.

The three example geometries reported in Fig. 8 have been designed following the just introduced flowchart. ***Design 1*** refers to distributed windings with q = 1, ***design 2*** is optimized for single layer windings with q = 2/5 (version 2*a*) and then re-evaluated with double layer windings (version 2*b*). Last, ***design 3*** is optimized for q = 2/5, double layer. All final designs have the same outer dimensions (stator diameter and stack length), the same calculated torque, and very similar Joule losses. Iron loss is not included in this analysis, due to the low fundamental frequency of all the design examples.

A. Design 1: distributed windings

The distributed winding example has q = 1. Higher numbers (q = 2, 3 ..) would make the slots too slender to be feasible. The geometry of *design 1* is described in Table I, along with its FEA evaluated performance. Table II compares the model results with FEA. The sketch of the laminations is on the left-hand side of Fig. 8.

The minimum inductance condition would have suggested a pole pitch factor $(a/g)_{Lmin}$ = 44.2 instead of the chosen a/g = 25.3. As said in subsection IV.C, the minimum inductance condition tends to be disadvantageous for distributed winding machines. *Design 1* here has p = 45 while one machine designed according to $(a/g)_{Lmin}$ would have had 25 pole pairs, and a significantly higher mass of the active parts. The power factor of *design 1* is still high enough (0.84 from the model, 0.85 from FEA). Moreover, the fundamental frequency is still low enough (12.7 Hz at rated speed) to assume that the iron and PM loss are negligible with respect to the Joule loss.

The tooth length of this machine (l_t/g = 30) is higher than the one of the other two machines of Fig. 8, having fractional slots. The teeth of *design 1* are necessarily longer to keep the Joule losses equal to the other designs. It is consistent with the literature that fractional slot machines have lower Joule losses due to their shorter end connections. This can be seen in (5), where the end winding factor k_{end} is in evidence. Besides, the two fractional slot machines also have a lower tooth scaling k_t factor (see Table I), and this again reduces the Joule loss according to (5). In other words, designs 2 and 3 have a more convenient slot to tooth split factor, resulting in a larger total copper area over the machine cross section. Also the slot filling factor k_{Cu} could be a matter of discussion, but here all examples have 0.4.

B. Design 2a: single layer, concentrated windings

The number of slots per pole per phase is q = 2/5, as suggested by all the considerations about the power factor, summarized in Figs. 5 to 7. The main data of *design 2* are in Table I, while the model versus FEA comparison is in Table III. The sketch of the laminations is in the middle of Fig. 8. As for *design 1*, the design flowchart is iterated for obtaining a stator radius that is exactly 2 m and to comply with the torque and loss targets. In this case, the pole pitch choice follows the minimum inductance condition (a/g = 19.3) and the corresponding pole pairs number is very close to 60, with no need of truncation. The model-calculated power factor is 0.7.

C. Design 2b: double layer version of design 2a

Design 2b is essentially the same machine of *design 2a*, where the single layer windings have been replaced by a set of double layer ones. Most of the data referring to this machine in Table I are the same given for *design 2a*. When different, the additional numbers in round brackets in the table refer to *design 2b*.

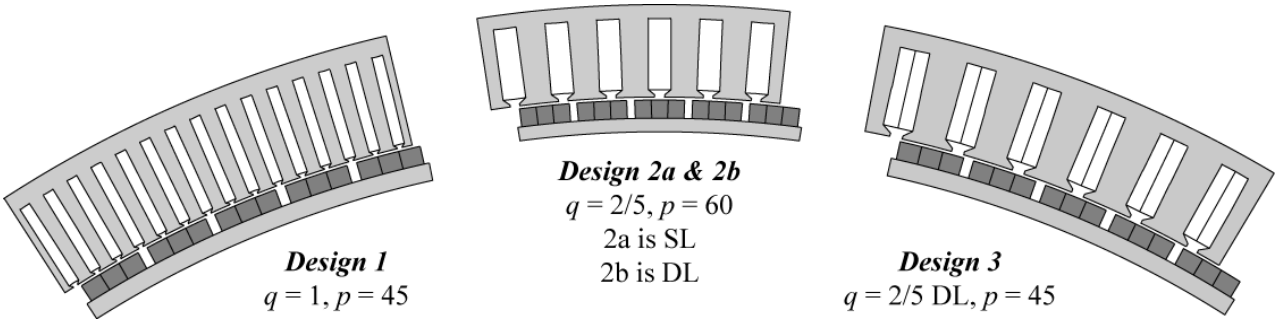

Figure 8. Sketches of the three design examples geometries.

TABLE I –MAIN DATA OF THE MACHINE DESIGN EXAMPLES

Design		***1***	***2***	***3***
Main input data				
Winding type		Dist	2a: SL (2b: DL)	DL
Slot/pole/phase	q	1	2/5	2/5
Airgap	g (mm)	5		
Magnet grade	B_r (T)	1.12		
PM length	l_m/g	6.1		
Core flux density	B_{fe} (T)	1.5		
Slot filling	k_{Cu}	0.4		
Stator radius	R (m)	2.00		
Design results				
Rotor radius	r (m)	1.807	1.840	1.815
Stack length	l (m)	1.3		
Pole pitch	a/g	25.3	19.3	25.4
Tooth length	l_t/g	30.4	23.8	26.6
Pole pairs	p	45	60	45
Carter	k_c	1.053	1.085	1.101
End connections	k_{end}	1.334	1.094 (1.066)	1.087
Tooth scaling	k_t	0.8	0.76	0.76
Mass of active parts	(tons)	33.2	26.7 (26.5)	29.5
Mass of PMs	(tons)	2.96	3.01	2.97
FEA evaluated performance				
Torque	(Nm)	1562	1533 (1572)	1609
Joule loss	(kW)	108	110 (118)	109
PF		0.85	0.70 (0.78)	0.78

Also, Table III reports the FEA to model comparison for this particular machine. In brief, the double layer version shows a significantly higher power factor (0.78 versus 0.70), but also a little increase of Joule losses for giving the same torque (118 kW versus 110 kW). This is due to the winding factor k_w that is lower with double layers (0.966 versus 0.933).

D. Design 3: double layer with optimized PF

Design 3 is also reported in Table I and in Fig. 8, on the right-hand side. Table IV reports the model and the FEA calculated performance. The number of poles has been chosen for inductance minimization according to (15) and (18), apart from pole-pair truncation. According to FEA, *design 3* is the one giving the highest torque, or the less underestimated one (1609 Nm against the target 1695 Nm), due to a lower impact of core saturation that will be discussed later. Joule losses are the same of *design 1* and *design 2a* and the weight of the active parts is intermediate between the three geometries. The power factor is practically equal to the one of *design 2b*, even if that machine was not specifically designed for PF maximization, in the double layer version. This could sound counterintuitive, in a way, but it must be considered that *design 3* has longer teeth, and then a PF factor that tends to be worse due to the slot leakage inductance.

Which solution is better between *design 2a* and *design 3* is a matter of discussion, the former being lighter (26.5 tons versus 29.5 tons), while the latter giving more torque for the same loss.

E. Finite element validation of the model

The per-unit design procedure has been validated via static magnetic FEA using FEMM [13]. Finite element results are given in Tables II to IV, next to the model results for the design examples. Both with the model and with FEA, the magnetic loading B is evaluated at no load, and the numbers are very alike in this case, for all machines. The model calculated target torque is purposely equal (1695 kNm), as well as the model calculated Joule loss (109 kW). The number of turns in series per phase is chosen to set the phase voltage of all machines to 577 V peak, at rated current. This calculation was based on FEA results. The discrepancy between FEA and model evaluated losses in the Tables is related to the effect of curvature on the actual cross section of the slots. It is no coincidence that this effect is more evident in *design 1*, which is the one with the longest teeth. In fact, the linear model underestimates the cross section of slots, and the approximation is always conservative

TABLE II – PERFORMANCE OF DESIGN 1, $q = 1$

	Eq.	Model	FEA
B (T)	(1)	1.10	1.10
A (A/m)	(3)	54293	
σ (kN/m^2)		63.22	58.25
T (kNm)	(16)	1695	1562
Phase Current (Apk)		3845	
Phase Voltage (Vpk)		636	577
Phase back-emf (Vpk)		518	518
Joule loss (kW)		119.2	107.9
L_g (mH)	(9)	0.274	
L_{slot} (mH)	(10)	0.683	
L_{tip} (mH)		0.137	
L_{tot} (mH)		1.09	1.05
PF		0.84	0.85

TABLE III – PERFORMANCE OF DESIGN 2, $q = 2/5$

		Single Layer		Double Layer	
	Eq.	Model	FEA	Model	FEA
B (T)	(1)	1.10	1.09	same	same
A (A/m)	(3)	55499		same	
σ (kN/m^2)		60.96	55.13	same	56.53
T (kNm)	(16)	1695	1533	same	1572
Phase Current (Apk)		4421		4233	
Phase Voltage (Vpk)		661	577	621	577
Phase back-emf (Vpk)		451	447	470	466
Joule loss (kW)		119	110	125	118
L_g (mH)	(13)	0.385		0.225	
L_{slot} (mH)	(14)	0.390		0.398	
L_{tip} (mH)		0.214		0.219	
L_{tot} (mH)		0.99	0.98	0.84	0.87
PF		0.7	0.72	0.78	0.77

TABLE IV – PERFORMANCE OF DESIGN 3, $Q = 2/5$

	Eq.	Model	FEA
B (T)	(1)	1.10	1.11
A (A/m)	(3)	57158	
σ (kN/m^2)		62.65	59.46
T (kNm)	(16)	1695	1609
Phase Current (Apk)		4286	
Phase Voltage (Vpk)		623	577
Phase back-emf (Vpk)		466	470
Joule loss (kW)		119	109
L_g (mH)	(13)	0.396	
L_{slot} (mH)	(14)	0.453	
L_{tip} (mH)		0.295	
L_{tot} (mH)		1.14	1.18
PF		0.77	0.78

VII. DISCUSSION OF OTHER EFFECTS

A. Tooth tip inductance

The ***tooth tip inductance*** term L_{tip} has been evaluated analytically in Tables II to IV, but its equation was not explicitly mentioned in the paper for the sake of simplicity. The tooth tip inductance requires a few additional parameters to be defined [10], and the tooth tip shape can vary a lot from case to case. The impact of the tooth tip term on the choice of the critical pole pitch $(a/g)_{Lmin}$ is very limited, and such simplification does not affect the final design, apart from the correct evaluation of the PF, that must include L_{tip}.

B. Steel saturation

The torque versus current curves in Fig. 9, FEA calculated, show the progressive effect of core saturation with current loading. The torque at rated current is lower than the one predicted by the per-unit model, that assumes magnetic linearity. In the presented modelling approach, the choice of the parameter B_{fe} determines the yoke and tooth widths. This is the target peak value of the flux density in the back iron, intended at no load. All the examples in the paper refer to B_{fe} = 1.5 T. The yokes of all the design examples are then expected to have peak flux densities of 1.5 T at no load, and that is confirmed by FEA. When at load, the stator core will actually work at higher flux densities, due to the armature flux, and then saturate progressively.

In Fig. 9, *design 2a* is the one suffering most from saturation. To a certain extent, those machines having a higher armature flux linkage (a lower power factor) are also more likely expected to have a torque reduction due to saturation. *Design 2a* is, in fact, the machine with the lowest power factor. The double layer version of the same machine, *design 2b*, has a better power factor and, consistently, a lower saturation.

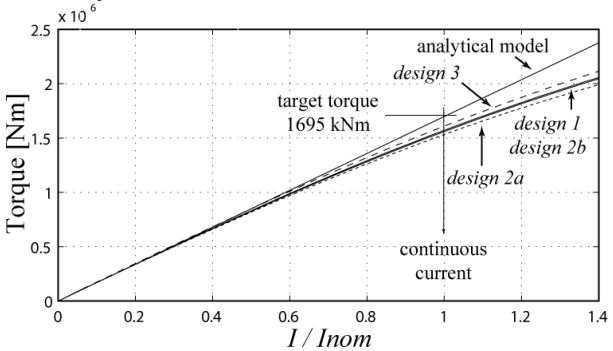

Figure 9. Machine torque according to the linear model and the FEA, as a function of the machine current, for the two designs, to put in evidence the effect of core saturation.

However, when coming to compare designs 1 and 3, it turns out that the one with the lower PF (*design 3* has 0.78 and *design 1* has 0.85) saturates less at rated current. This is related to the shorter tooth length of *design 3*. The model

could be modified to include saturation, but this has been avoided for simplicity. A possible countermeasure to reduce the torque overestimate, with no model complication, could be to oversize the yoke and tooth widths by a certain factor, by setting a lower no load peak flux density (e.g. B_{fe} = 1.4 T).

In Tables II to IV the phase voltage amplitude from the model and from FEA are different, again due to core saturation.

Last, the L_{tot} inductances in the tables are FEA calculated at low current loading, before saturation, to be comparable with the respective values given by the model.

C. Design maps at given outer dimensions

It is interesting to see how the design philosophy based on elementary blocks can partially change when moving to real world rotating machine. The blocks of the per-unit model refer to the airgap surface (radius r), that is not equal for all the designs at Section VI, where it is the outer dimension (R = 2 m) that is always the same, instead.

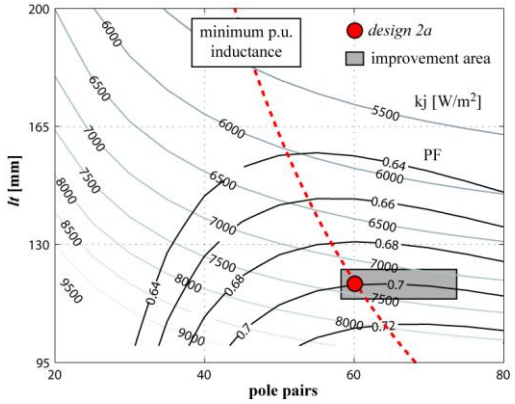

Figure 10. PF and W/m^2 countour curves at constant outer dimensions (R = 2m, l = 1.3m) and constant torque (1695 kNm), for q = 2/5, single layer.

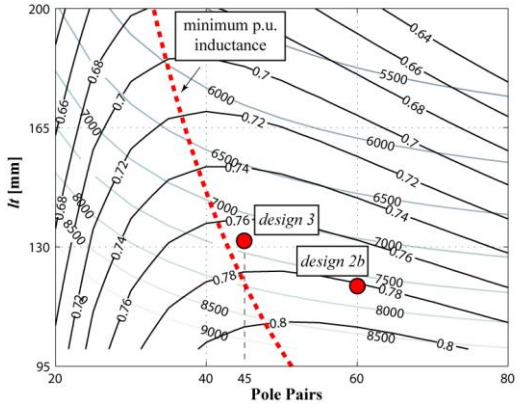

Figure 11. PF and W/m^2 countour curves at constant outer dimensions (R = 2m, l = 1.3m) and constant torque (1695 kNm), for q = 2/5, double layer.

Figs. 10 and 11 summarize the performance of a family of rotating machines all having the same stack cylinder (R = 2m, l = 1.3m) and the same output torque (1695 Nm). All the curves have been traced by means of the linear per-unit model, applied iteratively to obtain R = 2 m and the specified torque. All machines of Fig. 10 have q = 2/5, single layer, including *design 2a*, while Fig. 11 refers to q = 2/5, double layer (*design 2b* and *design 3*). The PF and the specific loss contour curves are reported as a function of the number of pole pairs and of the tooth length. The red dotted line represents the family of machines having the p.u. pole inductance minimized, that should be the ones with the best PF at given loss, according to the elementary blocks approach.

Fig. 10 shows that the loss of *design 2a*, which lays on the red line, can be reduced by increasing the number of poles and keeping the same tooth length. The gray "improvement area" indicates machines with a lower k_j and the PF substantially unchanged.

Similarly, *design 3* is on the red line in Fig. 11, apart from pole truncation to p = 45, and it can become more efficient again by moving horizontally in the graphs, still with a good PF. *Design 2b* is not red-line optimized, and yet its PF is higher than the one of *Design 3*, at the expense of higher Joule losses.

Dealing with the mass of the active parts, moving horizontally in Figs. 10 and 11 means to ***slightly reduce the total mass.*** This because machines with higher poles and same tooth length have a thinner back iron both in the stator and in the rotor.

To summarize, the red curve of minimum inductance splits the dominion of possible designs into a ***right-hand area of convenient designs*** and a left-hand area of non convenient designs. There are good reasons to choose to stay on the line or to move slightly rightwards, but there are no reasons for moving leftwards, because all figures of merit (PF, k_j, mass) would deteriorate in that case.

VIII. Conclusion

The design of surface mounted permanent magnet motors with high number of poles is approached by means of a per-unit analytical model, assuming magnetic linearity and a rectified geometry. The formulas cover distributed and concentrated windings, that are compared according to. An original expression for the airgap inductance is presented, valid for fractional windings of all slot/pole/phase combinations, single or double layer. It can be verified that the airgap inductance of a double layer winding machine is exactly one half of that of the corresponding single layer machine.

The PF maximization criterion, at continuous current loading, orientates the selection of the pole pitch and then the number of pole pairs. It is not to be respected strictly, but it splits bad designs from good designs.

The passage from the rectified to the cylindrical machine is addressed, as well as the effects of steel saturation, that are FEA quantified and commented.

Four design examples are presented, with reference to a large size, direct drive wind generator. The examples confirm that single layer, concentrate winding machines are at risk of an unfeasibly low PF, and that double layer ones are, instead, very flexible in setting the PF at the designer's will. Distributed winding machines must have longer teeth to keep up with the others in terms of Joule losses, and they are then the heaviest of all, when efficiency is constrained.

Iron loss is neglected here, but it could limit the feasible number of poles in applications having higher speeds. The single layer windings, that require higher pole numbers for giving the same PF of double layer ones, could be further penalized in this perspective.

REFERENCES

[1] Jahns, T.M.; "The expanding role of PM machines in direct-drive applications," Electrical Machines and Systems (ICEMS), 2011 International Conference on , vol., no., pp.1-6, 20-23 Aug. 2011

[2] EL-Refaie, A.M.; "Fractional-Slot Concentrated-Windings Synchronous Permanent Magnet Machines: Opportunities and Challenges," Industrial Electronics, IEEE Transactions on , vol.57, no.1, pp.107-121, Jan. 2010

[3] Mecrow, B.C.; Jack, A.G.; Haylock, J.A.; Coles, J.; , "Fault-tolerant permanent magnet machine drives," Electric Power Applications, IEE Proceedings - , vol.143, no.6, pp.437-442, Nov 1996

[4] Cros, J.; Viarouge, P.; , "Synthesis of high performance PM motors with concentrated windings ," Energy Conversion, IEEE Transactions on , vol.17, no.2, pp.248-253, Jun 2002

[5] Magnussen, F.; Sadarangani, C.; , "Winding factors and Joule losses of permanent magnet machines with concentrated windings," *Electric Machines and Drives Conference, 2003. IEMDC'03. IEEE International* , vol.1, no., pp. 333- 339 vol.1, 1-4 June 2003

[6] P. Salminen, Fractional Slot Permanent Magnet Synchronous Motors for Low Speed Applications. Dissertation, Lappeenranta University of Technology, 2004, p. 150.

[7] Bianchi, N.; Dai Pre, M.; , "Use of the star of slots in designing fractional-slot single-layer synchronous motors," Electric Power Applications, IEE Proceedings - , vol.153, no.3, pp. 459- 466, 1 May 2006

[8] El-Refaie, A.M.; Jahns, T.M.; Novotny, D.W.; , "Analysis of surface permanent magnet machines with fractional-slot concentrated windings," *Energy Conversion, IEEE Transactions on* , vol.21, no.1, pp. 34- 43, March 2006

[9] Ronghai Qu; Lipo, T.A.; , "General closed-form analytical expressions of air-gap inductances for surface-mounted permanent magnet and induction machines," Electric Machines and Drives Conference, 2003. IEMDC'03. IEEE International , vol.1, no., pp. 443- 448 vol.1, 1-4 June 2003

[10] D.W. Novotny and T. A. Lipo, "Vector Control and Dynamics of AC Drives", Oxford, U.K.: Calderon, 1998.

[11] Boazzo, B.; Pellegrino, G.; Vagati A.; , "Multipolar SPM machines for direct drive application: a comprehensive design approach", International Energy Conference & Exibition. Energycon 2012, 9-12 Sept. 2012.

[12] Rasmussen, K.F.; Davies, J.H.; Miller, T.J.E.; McGelp, M.I.; Olaru, M.; , "Analytical and numerical computation of air-gap magnetic fields in brushless motors with surface permanent magnets," Industry Applications, IEEE Transactions on , vol.36, no.6, pp. 1547- 1554, Nov/Dec 2000.

[13] D. C. Meeker, Finite Element Method Magnetics, Version 4.0.1 (03Dec2006 Build), http://www.femm.info

[14] Abdennadher, I.; Kessentini, R.; Masmoudi, A.; , "Analytical derivation and FEA validation of the inductances of CWPMM," Systems, Signals and Devices, 2009. SSD '09. 6th International Multi-Conference on , vol., no., pp.1-7, 23-26 March 2009

APPENDIX: MATHEMATICAL DERIVATION OF EQUATIONS (10),(13-14)

Airgap inductance of fractional slot machines (14)

The phase inductance, divided by the number of poles, accounts for self and mutual coupling contributions:

$$L_{g,pole} = \frac{1}{2p} \cdot \left(L_{g,aa} - M_{g,ab}\right) \qquad (19)$$

The two terms in (19) come from the integration of the winding functions N_a (phase a) and N_b (phase b) [10]:

$$L_{g,pole} = \frac{\mu_0 l \cdot a}{k_c g + l_m} \cdot \left[\frac{1}{2\pi} \cdot \left(\int_{-\pi}^{\pi} N_a^2 d\vartheta - \int_{-\pi}^{\pi} N_a N_b d\vartheta\right)\right] \quad (20)$$

Fractional slot windings can be grouped as in Table V, with all combinations belonging to one group having the same *a* and *b* winding functions. The "basic" slot and pole numbers represent one electric periodicity as defined in [7].

TABLE V – EXAMPLES OF WINDING FUNCTIONS INTEGRALS

q	*basic slots*	*basic poles*	*layers* (n_l)	$\frac{1}{2\pi}\int_{-\pi}^{\pi} N_a^2 d\vartheta$	$-\frac{1}{2\pi}\int_{-\pi}^{\pi} N_a N_b d\vartheta$	*total*
½	3	2	2	$\frac{N_{slot}^2}{18}$	$\frac{N_{slot}^2}{36}$	$\frac{N_{slot}^2}{12}$
¼		4				
1/8		8				
1/10		10				
½	6	4	1	$\frac{5}{36}N_{slot}^2$	$\frac{N_{slot}^2}{36}$	$\frac{N_{slot}^2}{6}$
¼		8				
1/8		16				
1/10		20				
3/8	9	8	2	$\frac{13N_{slot}^2}{4 \cdot 81}$	$\frac{N_{slot}^2}{8 \cdot 81}$	$\frac{N_{slot}^2}{12}$
3/10		10				
2/5	12	10	1	$\frac{N_{slot}^2}{6}$	0	$\frac{N_{slot}^2}{6}$
2/7		14	2	$\frac{N_{slot}^2}{12}$	0	$\frac{N_{slot}^2}{12}$

The arrangement of phase coils into slots is made according to [7], as well. Table V reports the result of the two integral terms in square brackets in (20). All the slot/pole examples have a winding factor equal or greater than 0.866, with the "basic slots" number limited to 12 for space reasons. It turns out that the sum of the winding integrals is always $N_{slot}^2/(6n_l)$. N_{slot} is the number of conductors per slot, that is also N/q. From (20) and Table V, finally:

$$L_{g,pole} = \frac{\mu_0 l \cdot a}{k_c g + l_m} \cdot \frac{1}{6n_l} \cdot \left(\frac{N}{q}\right)^2 \qquad (21)$$

The normalization of (21) by L_{base} (7) leads to (14).

Slot leakage inductance (10),(13)

Given one slot of rectangular shape, whose dimensions are l_t and w_{slot}, filled with N_{slot} conductors all belonging to the same phase, its leakage inductance is:

$$L_{1slot} = \frac{1}{3}\mu_0 \cdot l \cdot N_{slot}^2 \cdot \frac{l_t}{w_{slot}} \quad (22)$$

From the definitions in Fig. 1, the slot width is:

$$w_{slot} = \frac{a}{3q}\left(1-\frac{B}{B_{fe}}k_t\right) \quad (23)$$

The inductance of one machine pole is q times the one of one slot:

$$L_{slot,pole} = \mu_0 \cdot l \cdot N^2 \cdot \frac{l_t}{a} \cdot \frac{1}{1-\frac{B}{B_{fe}}k_t} \quad (24)$$

Where $N_{slot} = N/q$ and (23) have been substituted. The normalization by L_{base} (7) leads to (25), that is both equal to (10) and to (13) with $n_l = 1$.

$$L_{slot,pu,nl=1} = \frac{\pi^2}{2k_w^2} \cdot \frac{l_t}{a} \cdot \frac{1}{1-\frac{B}{B_{fe}}k_t} \quad (25)$$

In double layer windings, different phases are sharing the same slots. The effect of mutual inductances reduces the resulting pole inductance, as well described in [14]. In particular, the mutual term acts differently according to the phase difference of the currents that are sharing each slot. Again, testing all possible combinations, it turns out that the windings can be grouped according to Q_0, introduced at subsection III.A, and that the normalized per-pole inductance of a double layer machines is (26) times the one of a single layer machine, as in (13).

$$\frac{L_{slot,nl=2}}{L_{slot,nl=1}} = 1 - \frac{3}{4 \cdot Q_o} \quad (26)$$

For clarity, Table VI reports examples of Q_0.

TABLE VI – VALUES OF Q_0 FOR EXAMPLE DOUBLE LAYER COMBINATIONS

slots	3				9		12		15		18	
poles	2	4	8	10	4	8	10	14	14	16	14	22
Q_0	**3**				**9**		**6**		**15**		**9**	